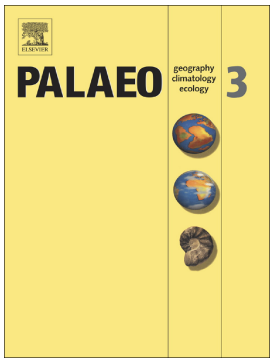

Evidence for volcanism and weathering during the Permian-Triassic mass extinction from Meishan (South China) osmium isotope record

Zeyang Liu, David Selby, Hua Zhang, Shuzhong Shen

PII: S0031-0182(20)30235-2

DOI: https://doi.org/10.1016/j.palaeo.2020.109790

Reference: PALAEO 109790

To appear in: *Palaeogeography, Palaeoclimatology, Palaeoecology*

Received date: 13 November 2019

Revised date: 29 January 2020

Accepted date: 3 May 2020

Please cite this article as: Z. Liu, D. Selby, H. Zhang, et al., Evidence for volcanism and weathering during the Permian-Triassic mass extinction from Meishan (South China) osmium isotope record, *Palaeogeography, Palaeoclimatology, Palaeoecology* (2019), https://doi.org/10.1016/j.palaeo.2020.109790

Evidence for volcanism and weathering during the Permian-Triassic mass extinction from Meishan (South China) osmium isotope record

Zeyang Liu[a], David Selby[a,d], Hua Zhang[b], Shuzhong Shen[c]

[a]Department of Earth Sciences, Durham University, Durham DH1 3LE, UK

[b]State Key Laboratory of Palaeobiology and Stratigraphy, Nanjing Institute of Geology and Palaeontology and Center for Excellence in Life and Paleoenvironment, Chinese Academy of Sciences, 39 East Beijing Road, Nanjing 210008, China

[c]State Key Laboratory of Mineral Deposits Research, Nanjing University and School of Earth Sciences and Engineering, Nanjing University, Nanjing, 210023, China

[d]State Key Laboratory of Geological Processes and Mineral Resources, School of Earth Resources, China University of Geosciences, Wuhan, 430074, Hubei, China

Corresponding author: Zeyang Liu (geozy.liu@outlook.com)

Abstract

The Permian–Triassic mass extinction event is the most severe biotic crisis during the Phanerozoic. The trigger of this event has been widely linked with massive volcanic activity associated with the Siberian Traps Large Igneous Province. However, the direct link is still lacking to fully understand the event. In this study, we apply osmium isotope ($^{187}Os/^{188}Os$, or Os_i) stratigraphy across the Permian–Triassic boundary interval in the Meishan section of South China. The Os isotope stratigraphy reveals multiple shifts to more unradiogenic $^{187}Os/^{188}Os$ composition that are interpreted to reflect pulses of volcanism across the mass extinction interval. Additionally, a shift to a more radiogenic $^{187}Os/^{188}Os$ composition is also found immediately above the mass extinction interval, which is taken to reflect the enhanced weathering of the continental crust in response to greenhouse gas release into the atmosphere and the associated hyperthermal.

Keywords: pulsed volcanism; rhenium; end-Permian; weatherability; Earth regulation mechanism

1 Introduction

The Permian–Triassic mass extinction is the most severe biotic crisis in the Phanerozoic era, eliminating almost 90 % marine biota and 75 % terrestrial species (e.g. Erwin, 2006). This event is marked by large negative carbon isotope excursions that indicate perturbations of the global carbon cycle (e.g. Korte and Kozur, 2010). It is associated with massive changes in the paleoclimate and palaeoceanography, including global warming (Joachimski et al., 2012; Sun et al., 2012; Chen et al., 2016), oceanic acidification (Hinojosa et al., 2012; Garbelli et al., 2017), anoxia and/or euxinia (Cao et al., 2009; Grice et al., 2005). The ultimate trigger has been commonly linked with intensive volcanism associated with the Siberian Traps Large Igneous Province (LIP) (Payne and Kump, 2007; Saunders and Reichow, 2009; Shen et al., 2013, 2019b; Burgess and Bowring, 2015; Svensen et al., 2009). This is supported by high-resolution U-Pb dating of volcanic tuff units in South China and volcanic rocks of the LIP (e.g. Burgess et al., 2014; Burgess and Bowring, 2015; Burgess et al., 2017; Shen et al., 2011), as well as other geochemical proxies (e.g. mercury [Hg] and zinc [Zn]; Liu et al., 2017; Wang et al., 2018, Shen et al., 2019a). Although intensive studies have investigated this catastrophic event, additional data from osmium isotope would be able to track the pattern of the volcanism and its temporal relationship with this great mass extinction event.

The seawater osmium (Os) isotope composition ($^{187}Os/^{188}Os$) reflects the balance of radiogenic input from weathering of ancient continent (~ 1.4) and unradiogenic input from mantle and extraterrestrial sources (~0.126) (Peucker-Ehrenbrink and Ravizza, 2000). The short oceanic residence time of osmium (≤10-50 kyr; e.g. Rooney et al., 2016; Peucker-Ehrenbrink and Ravizza, 2000) permits the ability of osmium isotopes to track short-periodic, yet globally averaged changes in the ocean. The osmium isotope can be captured and

preserved in the organic matter of sediments without isotope fractionation (Ravizza and Turekian, 1992). Thus, the paleo-seawater osmium isotope records can be reconstructed by analysing the initial osmium isotope compositions of sedimentary rocks (e.g. Cohen, 2004; Ravizza and Turekian, 1989; Turgeon and Creaser, 2008). In this study, we present osmium isotope stratigraphy on the Meishan section (South China) to provide further insights into the triggering mechanism of the mass extinction and the climate response of Earth system.

2 Geological background

The Meishan section (31°4'55" N, 119°42'22.9" E) is located in Changxing County, South China and contains the Global Stratotype Section and Points (GSSPs) for the Permian–Triassic boundary and the Wuchiapingian–Changhsingian boundary (Jin et al., 2006; Yin et al., 2001). The section records a middle-upper slope depositional setting (Fig. 1; Yin et al., 2001). The lithology of the section is micritic limestone of the lower Changhsing Formation, which is overlain by calcareous mudstone interbedded with limestone of the Yinkeng Formation (Fig. 2). This section is constrained by high-resolution biostratigraphy and CA-TIMS U-Pb zircon tuff ages (e.g. Burgess et al., 2014; Shen et al., 2011; Yuan et al., 2014). The Late Permian mass extinction event interval is defined to be between bed 24e and bed 28 (Shen et al., 2011; Burgess et al., 2014).

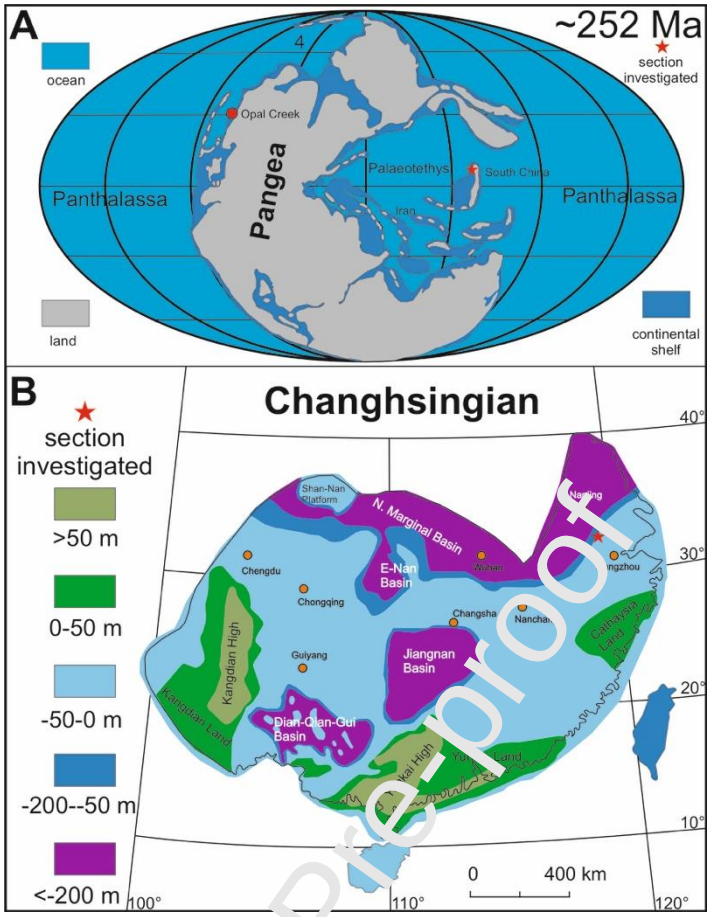

Figure 1. Late Permian paleogeographic maps showing the studied areas. (A) Changhsingian global paleogeographic reconstruction map showing the position of the studied section; base map after Ziegler et al. (1997). (B) South China; base map modified from Wang and Jin (2000). Figure modified from Liu et al. (2019).

3 Methods

Samples (n = 21) were collected from a drill core (Meishan-1, 550m to the west of the Meishan Section D) with increased sampling resolution across the P–T boundary (Cao et al., 2009). All samples were polished to eliminate contamination from cutting and drilling marks. The samples were then air dried at 60°C for ~12 hours, broken into chips with no metal contact. Samples were crushed to a fine powder (~30 μm) in a Zirconia ceramic dish using a shatterbox. The Re–Os isotope analysis were carried out at the Durham Geochemistry Centre (Laboratory for Sulfide and Source Rock Geochronology and Geochemistry, and Arthur

Holmes Laboratory) at Durham University. A Cr^{VI}–H_2SO_4 solution was utilized to preferentially digest the organic fraction of the samples and thus liberate hydrogenous Re and Os budget, minimising the contamination from detrital Re and Os (Selby and Creaser, 2003; Kendall et al., 2004). The sample powder (~ 1 g) together with a known amount of mixed ^{190}Os+^{185}Re tracer (spike) solution and 8 ml of 0.25 g/g Cr^{VI}–H_2SO_4 solution were digested in a sealed carius tube for 48 h at 220 °C (Selby and Creaser, 2003). Rhenium was isolated from the acid using NaOH–C_3H_6O solvent extraction and then purified by anion chromatography. Osmium was purified using solvent extraction ($CHCl_3$) and micro-distillation methods (Cohen and Waters, 1996; Birck et al., 1997). The isolated Re and Os fractions were loaded onto Ni and Pt filaments, respectively (Selby et al., 2007). Isotopic measurements were determined using a ThermoElectron TRITON mass spectrometer using static Faraday collection for Re and secondary electron multiplier in peak-hopping mode for Os. Total procedural blanks during this study were 13.8 ± 3.5 pg and 0.07 ± 0.06 pg (1σ S.D., n = 6) for Re and Os, respectively, with an average $^{187}Os/^{188}Os$ value of 0.30 ± 0.19 (n = 6).

The initial $^{187}Os/^{188}Os$ were calculated using the equation:

$$^{187}Os/^{188}Os_{initial} = {}^{187}Os/^{188}Os_{measured} - (^{187}Re/^{188}Os_{measured} \times (EXP(\lambda \times t) - 1)). \quad (1)$$

λ is ^{187}Re decay constant $1.666e^{-11}yr^{-1}$ (Smoliar et al., 1996), t is the depositional age. Here, the Os_i values are calculated using each sample's age estimated following Burgess et al. (2014), assuming a constant deposition rate between CA-TIMS U-Pb zircon dated ash beds.

4 Results

The Re and Os concentrations range from 0.1 to 57.8 ppb and 12 to 721 ppt (^{192}Os = ~4–232 ppt), respectively (Table S1). The Os_i values through beds 19–23 are similar within uncertainty (~0.5). The Os_i values then shift to an unradiogenic value of ~0.2 immediately before bed 24 which then recover to ~0.6, and then show two single-point shifts to less

radiogenic values (~0.2) within bed 24d and 26, that correlate with a large negative carbon isotope excursion (Burgess et al., 2014). The Os_i values then increase gradually across the Permian–Triassic boundary and reach a very radiogenic value of ~1.2. The Os_i values drop to ~1.0 and then exhibit another shift to an unradiogenic value of ~0.3 which then returns to more radiogenic values of ~0.7 at the top of the measured section.

The ^{192}Os values are generally low (~6–18 ppt) within beds 19–23 which then increase sharply to ~232 ppt in tandem with the unradiogenic Os_i value of ~0.2 in bed 23. The ^{192}Os values then fall to ~15 ppt with two more highly enriched samples of ~137 ppt and ~58 ppt that yield the two further unradiogenic Os_i excursions in Bed 24d and 26. The ^{192}Os values then remain low (4–7 ppt) and increase slightly to ~25 ppt up section (Fig. 2).

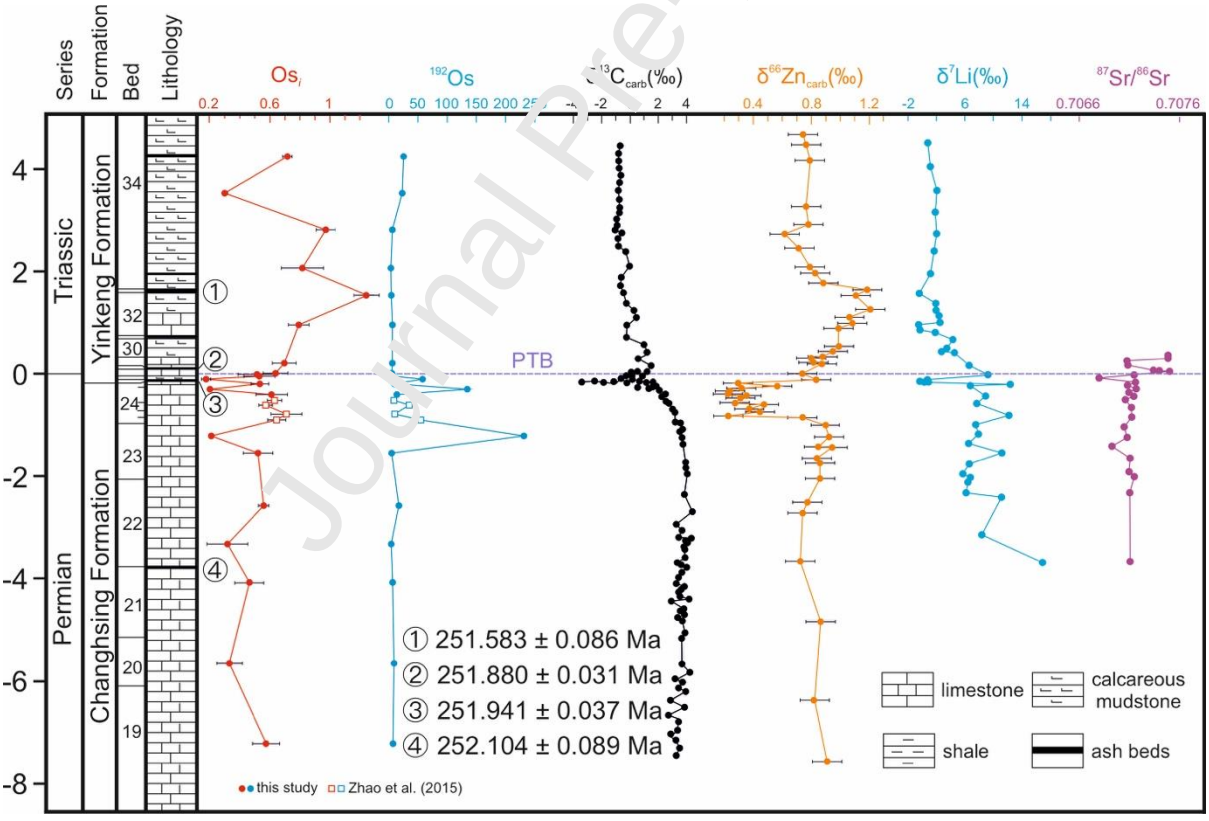

Figure 2. Carbon isotope (black), Os_i (red), ^{192}Os (blue), Zn isotope (orange), Li isotope (blue) and Sr isotope (purple) stratigraphy. The $\delta^{13}C_{carb}$ data are from Shen et al. (2011). Os data represented by a square symbol are from Zhao et al. (2015), Zn isotope data from Liu et

al. (2017), Li isotope data from Sun et al. (2018) and Sr isotope data from Song et al. (2015). Ages are from CA-TIMS U-Pb zircon dated volcanic ash beds (Burgess et al., 2014).

5 Discussion

5.1 Pulsed volcanism before, during and after the mass extinction event

The background Os_i values of ~0.5 – 0.6 of the Meishan section are comparable to the Late Permian seawater Os isotope values that reported from the P-T section at Opal Creek (Canada), Greenland and China (Georgiev et al., 2011, 2015; Schaefer et al., 2013; Yang et al., 2004). These Os_i values are also similar to the background Os_i values that are reported for the Wuchiapingian–Changhsingian boundary in South China and Canada (~2.2 Myr earlier; Liu et al., 2019). Three shifts to unradiogenic Os_i values are shown in this study (Fig. 2). The pattern and extent (from ~0.6 to ~0.2) of the excursions are comparable to that reported from Opal Creek (Georgiev et al., 2015). Additionally, this study also detected an unradiogenic shift in the Early Triassic which was not sampled in the Opal Creek section study (Fig. 3; Georgiev et al., 2015). This difference might be due to different sampling resolution. In theory, the shift to unradiogenic Os_i can be caused by increased input of unradiogenic Os from volcanism and/or meteorite impact (Peucker-Ehrenbrink and Ravizza, 2000). Furthermore, reduced weathering could also result in a shift to more unradiogenic Os_i, however, this is unlikely the case during a time of global warming such as that during the Late Permian (Chen et al., 2016). Based on the Os isotope data alone, we cannot rule out the possibility of meteorite impact events. However, there is no convincing evidence for an extraterrestrial impact during the Permian-Triassic boundary interval (Zhang et al., 2014). Even if the Os_i excursions are driven by meteorite impact, this would require four impact events, which would be very frequent considering such a short time interval (~400 kyr). Moreover, the spherules found from the Permian–Triassic boundary sections are interpreted

to be of biological, diagenetic and/or depositional origins or modern fly ash, rather than impact origin (Zhang et al., 2014). In contrast, several studies have demonstrated that intensive volcanic activity occurred throughout the Late Permian and Early Triassic (e.g. Burgess et al., 2014, 2017; Burgess and Bowring, 2015; Liu et al., 2017; Payne and Kump, 2007; Saunders and Reichow, 2009; Shen et al., 2019a, 2019b; Wang et al., 2018). The abrupt decline shown by Zn isotope values just below the mass extinction interval (bed 24) is interpreted to be caused by the rapid input of isotopically light zinc from volcanism, hydrothermal fluids and/or associated weathering of fresh LIPs (Liu et al., 2017). Therefore, in agreement with the interpretation of the previously reported Zn isotope data, we attribute the shifts to more unradiogenic Os isotope compositions to be associated with magmatic activity, possibly linked with the volcanism from South China (Georgiev et al., 2011; 2015; Korte and Kozur, 2010). At steady state, the seawater osmium isotope composition is determined by the mixing of radiogenic Os input (1.4) and unradiogenic Os input (0.12) given by:

$$R_{sw} = (M_u * R_u + M_r * R_r) \quad (1)$$

Where R_{sw}, R_u and R_r denote the Os isotope compositions of seawater, unradiogenic input and radiogenic input; M_u and M_r represent the mass of unradiogenic Os input and radiogenic Os input respectively. Assuming that the radiogenic input remained constant, to shift the Os data from 0.6 to 0.2 would require the unradiogenic Os input to the ocean to have increased by eight times.

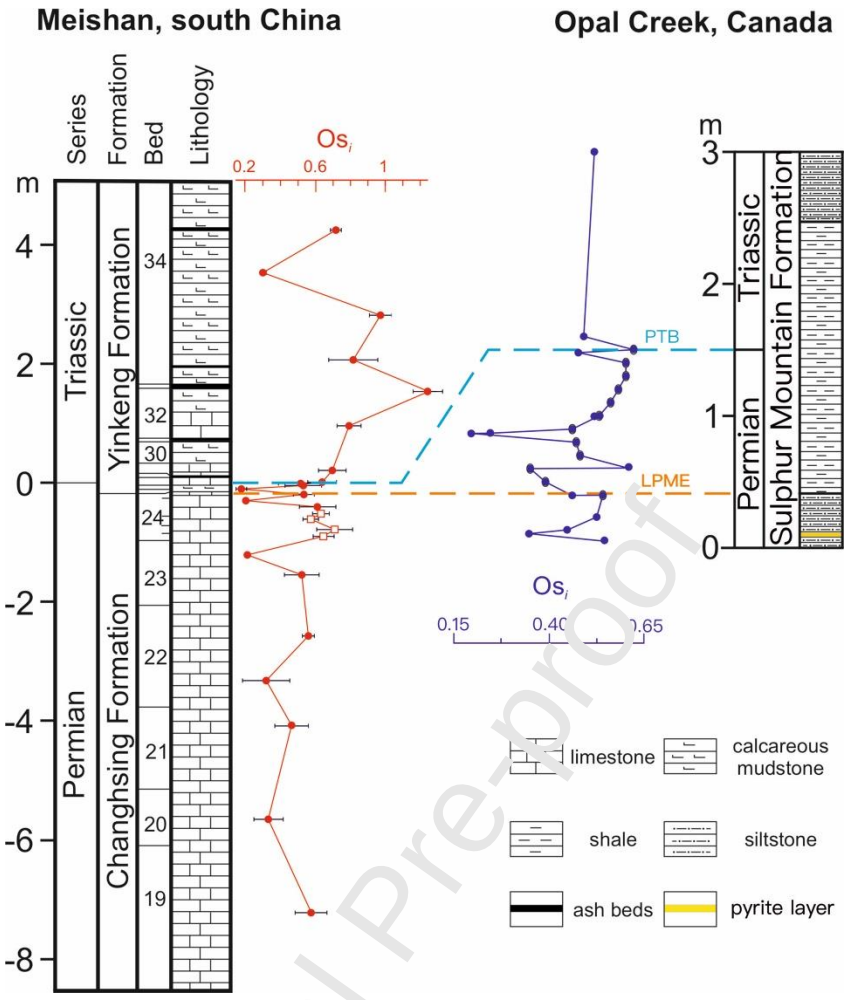

Figure 3. Figure showing the proposed correlation of Os isotope data from the Meishan section and the Opal Creek (Canada) section. The Opal Creek section data are from Georgiev et al. (2015).

Previously, the Permian–Triassic mass extinction event has been linked with large-scale volcanism based on high-precision U-Pb zircon ages and geochemistry proxies (e.g. Burgess et al., 2014; Burgess and Bowring, 2015; Grasby et al., 2016; Liu et al., 2017; Shen et al., 2011, 2019a; Wang et al., 2018). The Os isotope data here provide further insights into the pattern of the volcanism, and the temporal relationship between volcanic events and the mass extinction. Four unradiogenic shifts are inferred from the Os isotope data and this may indicate pulses of volcanism that occurred during the deposition of, 1) the upper part of bed 23; 2) bed 24d; 3) bed 26, and 4) bed 34 (Fig. 2). These unradiogenic Os_i shifts may correlate

to pulses of volcanism of South China and further support a causal link between volcanism and the Permian–Triassic mass extinction event (e.g. Burgess et al., 2014; Burgess and Bowring, 2015; Burgess et al., 2017). The abrupt shifts of seawater Os isotope values from ~0.6 to ~0.2 may suggest that the volcanism was pulsed and of a magnitude to disturb the global seawater Os isotope composition. The unradiogenic Os isotope shifts at bed 23 and 34 correlate to episodes of extrusive volcanism. Whereas the unradiogenic Os isotope shifts at bed 24d and 26 correlate to intrusive volcanism (Burgess et al., 2017).

5.2 Enhanced weathering after the mass extinction event

Large volcanic events are usually associated with greenhouse gas emission via direct outgassing and/or contact metamorphism that may rapidly escalate global temperature (e.g. Cui et al., 2011; Jenkyns, 2010). A negative feedback mechanism has been proposed for Earth to reduce the CO_2 and temperature through increased silicate/carbonate weathering feedback (Walker et al., 1981). One example of a hyperthermal event is the Paleocene–Eocene thermal maximum (PETM) event at 55.9 Ma (Charles et al., 2011). Global average temperature is suggested to have risen by about 5 °C during the PETM in response to thousands of gigatons of carbon injected into the atmosphere (3,000 – 10,000 Gt; Dunkley Jones et al., 2013; Gutjahr et al., 2017; Zachos et al., 2003). The weathering flux of terrestrial Os is suggested to have increased by ~40 % (Dickson et al., 2015). Global temperatures took ~200 kyr to return to pre-event levels (Katz et al., 1999). For the Permian–Triassic mass extinction event, a total of 30,000 – 40,000 Gt carbon is estimated to have been emitted (Cui and Kump, 2015), alongside a global temperature rise of between 8 and 16 °C (Joachimski et al., 2012; Chen et al., 2016). The Early Triassic Os_i data of this study show an overall increase from ~0.6 to ~0.9 from bed 27 to 34, with a one-point excursion to ~1.2 in bed 33 (Fig. 2). The increase in Os_i also coincides with the period of sea level rise (Cao et al., 2009; Yin et al., 2014). The increase in Os_i is interpreted to reflect an increase in radiogenic Os

input from enhanced weathering of the continent (Cohen et al., 2004). In theory, this radiogenic Os isotope excursion may also be caused by reduced unradiogenic Os input into the ocean. However, this scenario is very unlikely during a period of intensive and widespread volcanism (Peucker-Ehrenbrink and Ravizza, 2000). Assuming a constant unradiogenic Os input, a mass balance calculation using formula (1) indicates an approximate nine-fold increase in the weathering rate compared to the pre-event level (Dickson et al., 2015). Moreover, considering the possibly increased unradiogenic Os input from weathering of the fresh volcanic rock, the weathering rate could have increased even more. The increase in the Os_i coincides with a rise in Zn isotope compositions, with the peak Os_i value of 1.2 occurring alongside the peak in the Zn isotope composition (Fig. 2). The increase in the Zn isotope composition is interpreted to be caused by high primary productivity and/or enhanced sulphide burial that preferentially utilizes isotopically light Zn, possibly in response to high nutrition input and expanded ocean anoxia from enhanced weathering (Fig. 2; Liu et al., 2017). This interpretation is further supported by the Os_i data of this study and also by other proxies, such as lithium and strontium isotopes reported for the Meishan section (e.g. Song et al., 2015; Sun et al., 2018; Dudás et al., 2017). Carbonate Sr isotope records show increased $^{87}Sr/^{86}Sr$ values during the latest Permian, and this is interpreted to be caused by enhanced fluvial Sr input or reduced hydrothermal flux (Song et al., 2015; Dudás et al., 2017). Increased riverine Li input (with low δ^7Li values) from enhanced weathering is applied to explain the reported δ^7Li decrease during the latest Permian (Sun et al., 2018).

As mentioned above, Earth has the negative feedback mechanism to regulate the high temperature through enhanced silicate/carbonate weathering (Walker et al., 1981). The onset of advanced weathering during the earliest Triassic is discussed to have continued for a further 5 Myr (ca. 252-247 Ma). However, this interval still had a prolonged period of climate warming. This enhanced weathering during a period of prolonged warming is

considered to indicate a failed Earth regulation mechanism (Sun et al., 2012; Kump, 2018). The ultimate decline in the Earth's weatherability is considered to have been related to the development of a thick soil (Kump, 2018). A further possible scenario is that the majority of the weathered material is organic-rich (e.g. organic-rich sedimentary units) that typically possesses a radiogenic Os isotope composition and is more easily weathered (Peucker-Ehrenbrink and Hannigan, 2000). The weathering of shale alone may result in a net input of CO_2 into the atmosphere or hamper the consumption of CO_2 by silicate/carbonate weathering (Dickson et al., 2015; Ravizza et al., 2001). This emphasizes the need of further studies to fully understand the relationship between weathering processes and CO_2 draw down.

6 Conclusions

New Os isotope stratigraphy across the Permian–Triassic boundary interval of the Meishan section suggests episodes of volcanism before, during and after the mass extinction event and indicates a causal link between volcanism and the mass extinction event. The radiogenic Os isotope shift in the Early Triassic provides evidence of enhanced weathering rate in response to the massive CO_2 released from the volcanic activity. Further studies are needed to fully understand the full Earth system response to climate changes.

Data availability

Datasets related to this article can be found at https://data.mendeley.com, an open-source online data repository hosted at Mendeley Data (Liu et al., 2019).

Acknowledgements

ZL is grateful for the help provided by Wei Zhou in sampling the core and analytical support from Antonia Hofmann, Chris Ottley and Geoff Nowell. This work was supported by the Strategic Priority Research Program (B) of CAS (XDB26000000, XDB18000000). We gratefully acknowledge the financial support of the TOTAL Endowment Fund and the CUG

Wuhan Dida Scholarship to DS, and the University of Durham and China Scholarship Council to ZL.

References

Burgess, S. D., Bowring, S., and Shen, S.Z., 2014. High-precision timeline for Earth's most severe extinction. Proceedings of the National Academy of Sciences 111, 3316-3321.

Burgess, S. D., and Bowring, S. A., 2015. High-precision geochronology confirms voluminous magmatism before, during, and after Earth's most severe extinction. Science Advances 1.

Burgess, S. D., Muirhead, J. D., and Bowring, S. A., 2017. Initial pulse of Siberian Traps sills as the trigger of the end-Permian mass extinction. Nature Communications 8, 164.

Birck, J.L., Barman, M.R., Capmas, F., 1997. Re-Os isotopic measurements at the femtomole level in natural samples. Geostandards Newsletter 21, 19-27.

Cao, C.Q., Love, G. D., Hays, L. E., Wang, W., Shen, S.Z., and Summons, R. E., 2009. Biogeochemical evidence for euxinic oceans and ecological disturbance presaging the end-Permian mass extinction event. Earth and Planetary Science Letters 281, 188-201.

Charles, A. J., Condon, D. J., Harding, I. C., Pälike, H., Marshall, J. E. A., Cui, Y., Kump, L., and Croudace, I. W., 2011. Constraints on the numerical age of the Paleocene-Eocene boundary. Geochem. Geophys. Geosyst. 12, Q0AA17.

Chen, J., Shen, S.Z., Li, X.H., Xu, Y.G., Joachimski, M. M., Bowring, S. A., Erwin, D. H., Yuan, D.X., Chen, B., Zhang, H., Wang, Y., Cao, C.Q., Zheng, Q.F., and Mu, L., 2016. High-resolution SIMS oxygen isotope analysis on conodont apatite from South China and implications for the end-Permian mass extinction. Palaeogeography, Palaeoclimatology, Palaeoecology 448, 26-38.

Cohen, A. S., 2004. The rhenium–osmium isotope system: applications to geochronological and palaeoenvironmental problems. Journal of the Geological Society 161, 729-734.

Cohen, A. S., Coe, A. L., Harding, S. M., and Schwark, L., 2004. Osmium isotope evidence for the regulation of atmospheric CO_2 by continental weathering. Geology 32, 157-160.

Cohen, A.S., Waters, F.G., 1996. Separation of osmium from geological materials by solvent extraction for analysis by thermal ionisation mass spectrometry. Analytica Chimica Acta 332, 269-275.

Cui, Y., Kump, L. R., Ridgwell, A. J., Charles, A. J., Junium, C. K., Diefendorf, A. F., Freeman, K. H., Urban, N. M., and Harding, I. C., 2011. Slow release of fossil carbon during the Palaeocene–Eocene Thermal Maximum. Nature Geoscience 4, 481.

Cui, Y., and Kump, L. R., 2015. Global warming and the end-Permian extinction event: Proxy and modeling perspectives. Earth-Science Reviews 149, 5-22.

Dickson, A. J., Cohen, A. S., Coe, A. L., Davies, M., Shcherbinina, E. A., and Gavrilov, Y. O., 2015. Evidence for weathering and volcanism during the PETM from Arctic Ocean and Peri-Tethys osmium isotope records. Palaeogeography, Palaeoclimatology, Palaeoecology 438, 300-307.

Dudás, F. Ö., Yuan, D. X., Shen, S. Z., and Bowring, S. A., 2017. A conodont-based revision of the $^{87}Sr/^{86}Sr$ seawater curve across the Permian-Triassic boundary. Palaeogeography, Palaeoclimatology, Palaeoecology 470, 40-53.

Dunkley Jones, T., Lunt, D. J., Schmidt, D. N., Ridgwell, A., Sluijs, A., Valdes, P. J., and Maslin, M., 2013. Climate model and proxy data constraints on ocean warming across the Paleocene–Eocene Thermal Maximum. Earth-Science Reviews 125, 123-145.

Erwin, D. H., 2006. Extinction: how life on earth nearly ended 250 million years ago, Princeton University Press.

Garbelli, C., Angiolini, L., and Shen, S.Z., 2017. Biomineralization and global change: A new perspective for understanding the end-Permian extinction. Geology 45, 19-22.

Georgiev, S., Stein, H. J., Hannah, J. L., Bingen, B., Weiss, H. M., and Piasecki, S., 2011. Hot acidic Late Permian seas stifle life in record time. Earth and Planetary Science Letters 310, 389-400.

Georgiev, S., Stein, H. J., Hannah, J. L., Weiss, H. M., Bingen, B., Xu, G., Rein, E., Hatlø, V., Løseth, H., Nali, M., and Piasecki, S., 2012. Chemical signals for oxidative weathering predict Re–Os isochroneity in black shales, East Greenland. Chemical Geology 324-325, 108-121.

Georgiev, S. V., Stein, H. J., Hannah, J. L., Henderson, C. M., and Algeo, T. J., 2015. Enhanced recycling of organic matter and Os-isotopic evidence for multiple magmatic or meteoritic inputs to the Late Permian Panthalassic Ocean, Opal Creek, Canada. Geochimica et Cosmochimica Acta 150, 192-210.

Grasby, S. E., Beauchamp, B., Bond, D. P. G., Wignall, P. B., and Sanei, H., 2016. Mercury anomalies associated with three extinction events (Capitanian Crisis, Latest Permian Extinction and the Smithian/Spathian Extinction) in NW Pangea. Geological Magazine 153, 285-297.

Grice, K., Cao, C.Q., Love, G. D., Böttcher, M. E., Twitchett, R. J., Grosjean, E., Summons, R. E., Turgeon, S. C., Dunning, W., and Jin, Y.G., 2005. Photic Zone Euxinia During the Permian-Triassic Superanoxic Event. Science 307, 706-709.

Gutjahr, M., Ridgwell, A., Sexton, P. F., Anagnostou, E., Pearson, P. N., Pälike, H., Norris, R. D., Thomas, E., and Foster, G. L., 2017. Very large release of mostly volcanic carbon during the Palaeocene–Eocene Thermal Maximum. Nature 548, 573.

Hinojosa, J. L., Brown, S. T., Chen, J., DePaolo, D. J., Paytan, A., Shen, S.Z., and Payne, J. L., 2012. Evidence for end-Permian ocean acidification from calcium isotopes in biogenic apatite. Geology 40, 743-746.

Jaffe, L. A., Peucker-Ehrenbrink, B., and Petsch, S. T., 2002. Mobility of rhenium, platinum group elements and organic carbon during black shale weathering. Earth and Planetary Science Letters 198, 339-353.

Jenkyns, H. C., 2010. Geochemistry of oceanic anoxic events. Geochemistry Geophysics Geosystems 11.

Jin, Y.G., Wang, Y., Henderson, C.M., Wardlaw, B. R., Shen, S.Z., and Cao, C.Q., 2006. The Global Boundary Stratotype Section and Point (GSSP) for the base of Changhsingian Stage (Upper Permian). Episodes 29, 175-182.

Joachimski, M. M., Lai, X.L., Shen, S.Z., Jiang, H.S., Luo, G.M., Chen, B., Chen, J., and Sun, Y.D., 2012. Climate warming in the latest Permian and the Permian–Triassic mass extinction. Geology 40, 195-198.

Katz, M. E., Pak, D. K., Dickens, G. R., and Miller, K. G., 1999. The Source and Fate of Massive Carbon Input During the Latest Paleocene Thermal Maximum. Science 286, 1531-1533.

Kendall, B.S., Creaser, R.A., Ross, G.M., Selby, D., 2004. Constraints on the timing of Marinoan "Snowball Earth" glaciation by 187Re–187Os dating of a Neoproterozoic, post-glacial black shale in Western Canada. Earth and Planetary Science Letters 222, 729-740.

Korte, C., and Kozur, H. W., 2010. Carbon-isotope stratigraphy across the Permian–Triassic boundary: A review. Journal of Asian Earth Sciences 39, 215-235.

Liu, S.A., Wu, H.C., Shen, S.Z., Jiang, G.Q., Zhang, S.H., Lv, Y., Zhang, H., and Li, S.G., 2017. Zinc isotope evidence for intensive magmatism immediately before the end-Permian mass extinction. Geology 45, 343-346.

Liu, Z.Y., Selby, D., Zhang, H., Zheng, Q.F., Shen, S.Z., Sageman, B. B., Grasby, S. E., and Beauchamp, B., 2019. Osmium-isotope evidence for volcanism across the Wuchiapingian–Changhsingian boundary interval. Chemical Geology 529, 119313.

Payne, J. L., and Kump, L. R., 2007. Evidence for recurrent Early Triassic massive volcanism from quantitative interpretation of carbon isotope fluctuations. Earth and Planetary Science Letters 256, 264-277.

Peucker-Ehrenbrink, B., and Hannigan, R., 2000. Effects of black shale weathering on the mobility of rhenium and platinum group elements. Geology 28, 475-478.

Peucker-Ehrenbrink, B., and Ravizza, G., 2000. The marine osmium isotope record. Terra Nova 12, 205-219.

Ravizza, G., Norris, R. N., Blusztajn, J., and Aubry, M. P., 2001. An osmium isotope excursion associated with the Late Paleocene thermal maximum: Evidence of intensified chemical weathering. Paleoceanography 16, 155-163.

Ravizza, G., and Turekian, K. K., 1989. Application of the ^{187}Re-^{187}Os system to black shale geochronometry. Geochimica et Cosmochimica Acta 53, 3257-3262.

Ravizza, G., Turekian, K.K., 1992. The osmium isotopic composition of organic-rich marine sediments. Earth and Planetary Science Letters 110, 1-6.

Rooney, A. D., Selby, D., Lloyd, J. M., Roberts, D. H., Lückge, A., Sageman, B. B., and Prouty, N. G., 2016. Tracking millennial-scale Holocene glacial advance and retreat using osmium isotopes: Insights from the Greenland ice sheet. Quaternary Science Reviews 138, 49-61.

Saunders, A., and Reichow, M., 2009. The Siberian Traps and the End-Permian mass extinction: a critical review. Chinese Science Bulletin 54, 20-37.

Schoepfer, S. D., Henderson, C. M., Garrison, G. H., Foriel, J., Ward, P. D., Selby, D., Hower, J. C., Algeo, T. J., and Shen, Y., 2013. Termination of a continent-margin

upwelling system at the Permian–Triassic boundary (Opal Creek, Alberta, Canada). Global and Planetary Change 105, 21-35.

Selby, D., and Creaser, R. A., 2003. Re–Os geochronology of organic rich sediments: an evaluation of organic matter analysis methods. Chemical Geology 200, 225-240.

Selby, D., Creaser, R. A., and Fowler, M. G., 2007. Re–Os elemental and isotopic systematics in crude oils. Geochimica et Cosmochimica Acta 71, 378-386.

Shen, J., Algeo, T. J., Hu, Q., Xu, G.Z., Zhou, L., and Feng, Q.L., 2013. Volcanism in South China during the Late Permian and its relationship to marine ecosystem and environmental changes. Global and Planetary Change 105, 121-134.

Shen, J., Chen, J., Algeo, T. J., Yuan, S., Feng, Q.L., Yu, J., Zhou, L., O'Connell, B., and Planavsky, N. J., 2019a. Evidence for a prolonged Permian–Triassic extinction interval from global marine mercury records. Nature Communications 10, 1563.

Shen, S.Z., Ramezani, J., Chen, J., Cao, C.Q., Erwin, D.H., Zhang, H., Xiang, L., Schoepfer, S.D., Henderson, C.M., Zheng, Q.F., A. Bowring, S.A., Wang, Y., Li, X.H., Wang, X.D., Yuan, D.X., Zhang, Y.C., Lin, M., Wang, J., and Wu, Y. S., 2019b. A sudden end-Permian mass extinction in South China. GSA Bulletin 131, 205-223.

Shen, S.Z., Zhang, H., Zhang, Y.C., Yuan, D.X., Chen, B., He, W.H., Mu, L., Lin, W., Wang, W., Chen, J., Wu, Q., Cao, C.Q., Wang, Y., and Wang, X.D., 2019c. Permian integrative stratigraphy and timescale of China. Science China-Earth Sciences 62, 154-188.

Shen, S.Z., Crowley, J. L., Wang, Y., Bowring, S. A., Erwin, D. H., Sadler, P. M., Cao, C.Q., Rothman, D. H., Henderson, C. M., Ramezani, J., Zhang, H., Shen, Y., Wang, X.D., Wang, W., Mu, L., Li, W.Z., Tang, Y.G., Liu, X.L., Liu, L.J., Zeng, Y., Jiang, Y.F., and Jin, Y.G., 2011. Calibrating the End-Permian Mass Extinction. Science 334, 1367-1372.

Smoliar, M. I., Walker, R. J., and Morgan, J. W., 1996. Re-Os ages of group IIA, IIIA, IVA, and IVB iron meteorites. Science 271, 1099.

Svensen, H., Planke, S., Polozov, A.G., Schmidbauer, N., Corfu, F., Podladchikov, Y.Y. and Jamtveit, B., 2009. Siberian gas venting and the end-Permian environmental crisis. Earth and Planetary Science Letters, 277, 490-500.

Song, H.J., Wignall, P. B., Tong, J.N., Song, H.Y., Chen, J., Chu, D.L., Tian, L., Luo, M., Zong, K., Chen, Y., Lai, X.L., Zhang, K.X., and Wang, H., 2015. Integrated Sr isotope variations and global environmental changes through the Late Permian to early Late Triassic. Earth and Planetary Science Letters 424, 140-147.

Sun, H., Xiao, Y.L., Gao, Y.J., Zhang, G.J., Casey, J. F., and Shen, Y.A., 2018. Rapid enhancement of chemical weathering recorded by extremely light seawater lithium isotopes at the Permian–Triassic boundary. Proceedings of the National Academy of Sciences 115, 3782-3787.

Sun, Y.D., Joachimski, M. M., Wignall, P. B., Yan, C.L., Chen, Y.L., Jiang, H.S., Wang, L., and Lai, X.L., 2012. Lethally Hot Temperatures During the Early Triassic Greenhouse. Science 338, 366-370.

Them, T. R., Gill, B. C., Selby, D., Gröcke, D. R., Friedman, R. M., and Owens, J. D., 2017. Evidence for rapid weathering response to climatic warming during the Toarcian Oceanic Anoxic Event. Scientific Reports 7, 5003.

Turgeon, S. C., and Creaser, R. A., 2008. Cretaceous oceanic anoxic event 2 triggered by a massive magmatic episode. Nature 454, 323-326.

Walker, J. C. G., Hays, P. B., and Kasting, J. F., 1981. A negative feedback mechanism for the long-term stabilization of Earth's surface temperature. Journal of Geophysical Research: Oceans 86, 9776-9782.

Wang, X.D., Cawood, P. A., Zhao, H., Zhao, L.S., Grasby, S. E., Chen, Z.Q., Wignall, P. B., Lv, Z.Y., and Han, C., 2018. Mercury anomalies across the end Permian mass extinction in South China from shallow and deep water depositional environments. Earth and Planetary Science Letters 496, 159-167.

Wang, Y., and Jin, Y.G., 2000. Permian palaeogeographic evolution of the Jiangnan Basin, South China. Palaeogeography, Palaeoclimatology, Palaeoecology 160, 35-44.

Yang, G., Chen, J.F., Du, A.D., Qu, W.J., and Yu, G., 2004. Re-Os dating of Mo-bearing black shale of the Laoyaling deposit, Tongling, Anhui Province, China. Chinese Science Bulletin 49, 1396-1400.

Yin H.F., Zhang, K.X., Tong, J.N., Yang, Z.Y. and Wu, S.B., 2001. The Global Stratotype Section and Point (GSSP) of the Permian-Triassic Boundary. Episodes 24, 102-114.

Yin, H.F., Jiang, H.S., Xia, W.C., Feng, Q.L., Zhang, N., and Shen, J., 2014, The end-Permian regression in South China and its implication on mass extinction: Earth-Science Reviews, v. 137, p. 19-33.

Yuan, D.X., Shen, S.Z., Henderson, C. M., Chen, J., Zhang, H., and Feng, H.Z., 2014. Revised conodont-based integrated high-resolution timescale for the Changhsingian Stage and end-Permian extinction interval at the Meishan sections, South China. Lithos 204, 220-245.

Zachos, J. C., Wara, M. W., Bohaty, S., Delaney, M. L., Petrizzo, M. R., Brill, A., Bralower, T. J., and Premoli-Silva, I., 2003. A Transient Rise in Tropical Sea Surface Temperature During the Paleocene-Eocene Thermal Maximum. Science 302, 1551-1554.

Zhang, H., Shen, S.Z., Cao, C.Q., and Zheng, Q.F., 2014. Origins of microspherules from the Permian–Triassic boundary event layers in South China. Lithos 204, 246-257.

Zhao, H., Li, C., Jiang, X.J., Zhou, L.M., Li, X.W., Qu, W.J. and Du, A.D., 2015. Enrichment Mechanism of Re-Os in Limestone from Changxing Permian-Triassic Boundary in Zhejiang. Acta Geologica Sinica 89, 1783-1791. (in Chinese)

Ziegler, A.M., Hulver, M.L., Rowley, D.B., 1997. Permian world topography and climate. In: Martini, I.P. (Ed.), Late Glacial and Postglacial Environmental Changes–Quaternary, Carboniferous–Permian and Proterozoic. Oxford University Press, New York, 111-146.

Highlights

- Presented is Os isotope stratigraphy of the Meishan Permian–Triassic interval.
- Multiple unradiogenic Os isotope shifts are suggested to reflect pulses of volcanism.
- A radiogenic Os isotope excursion is found above the mass extinction interval.
- The radiogenic Os isotope shift may indicate enhanced weathering of the continent.